Advances in Applied Mathematics and Mechanics
Adv. Appl. Math. Mech., Vol. **1**, No. 1, pp. 29-55 (2009)

February 2009

Numerical Studies of Vanka-Type Smoothers in Computational Solid Mechanics

Hilmar Wobker[1,*] and Stefan Turek[1]

[1] *Institute of Applied Mathematics, LS3, TU Dortmund, D-44227 Dortmund, Germany.*

Received 27 November 2008; Accepted (in revised version) 5 January 2009
Available online 16 February 2009

Abstract. In this paper multigrid smoothers of Vanka-type are studied in the context of Computational Solid Mechanics (CSM). These smoothers were originally developed to solve saddle-point systems arising in the field of Computational Fluid Dynamics (CFD), particularly for incompressible flow problems. When treating (nearly) incompressible solids, similar equation systems arise so that it is reasonable to adopt the 'Vanka idea' for CSM. While there exist numerous studies about Vanka smoothers in the CFD literature, only few publications describe applications to solid mechanical problems. With this paper we want to contribute to close this gap. We depict and compare four different Vanka-like smoothers, two of them are oriented towards the stabilised equal-order Q_1/Q_1 finite element pair. By means of different test configurations we assess how far the smoothers are able to handle the numerical difficulties that arise for nearly incompressible material and anisotropic meshes. On the one hand, we show that the efficiency of *all* Vanka-smoothers heavily depends on the proper parameter choice. On the other hand, we demonstrate that only *some* of them are able to robustly deal with more critical situations. Furthermore, we illustrate how the enclosure of the multigrid scheme by an outer Krylov space method influences the overall solver performance, and we extend all our examinations to the nonlinear finite deformation case.

AMS subject classifications: 65N22, 65N55, 65H10, 65F50, 74S05

Key words: Coupled multigrid, Vanka smoother, linear and finite elasticity, nearly incompressible material, saddle point systems, finite elements.

1 Introduction

Multigrid solvers rank among the most efficient solvers in many application fields. They are especially suited for solving large linear equation systems stemming from

*Corresponding author.
URL: `http://www.mathematik.tu-dortmund.de/lsiii`
Email: `hilmar.wobker@math.tu-dortmund.de` (H. Wobker), `Stefan.Turek@math.tu-dortmund.de` (S. Turek)

discretisations of elliptic partial differential equations. In this paper we deal with such systems arising in the context of Computational Solid Mechanics (CSM). The continuous problems are discretised using the Finite Element method.

The efficiency and the robustness of the (geometric) multigrid method crucially depends on the smoothing operator. We want to examine a class of smoothers which was originally introduced by Vanka [35] for solving the Navier-Stokes equations discretised by Finite Differences. Basically, the method can be described as a block Gauß-Seidel iteration, which locally couples all field variables occuring in the formulation. The smoother is sometimes denoted as *symmetrically coupled Gauß-Seidel (SCGS)* or *box iteration/relaxation*. Compared to standard (point-wise) Jacobi or Gauß-Seidel smoothers, the crucial advantage of the Vanka approach is the ability to deal with zero blocks appearing on the diagonal of the system matrix. Saddle point systems stemming from discretisations of the incompressible Navier-Stokes equations have this property which is the main reason for the strong influence the method had (and still has) in the field of Computational Fluid Dynamics (CFD). Other reasons are that it is not too difficult to implement and at the same time efficient and robust for a wide class of problem configurations.

The Vanka approach has to be seen in contrast to the class of multigrid smoothers which treat the system in a global (and eventually decoupled) manner [8,24,32]. For a comparison between the different approaches in the context of CFD see, for example, the contributions of John, Tobiska [12, 15] and Turek [32]. For further references, see the overview paper of Wesseling and Oosterlee [36].

While there seem to be only few papers dealing with theoretical aspects of the smoother [20, 21, 29], much literature can be found presenting numerical studies of different Vanka-type smoothers for solving the discretised Navier-Stokes equations in CFD. John and Tobiska apply it to the non-conforming Crouzeix/Raviart element P_1/P_0, Turek to the corresponding non-conforming rotated bilinear Rannacher/Turek element $\tilde{Q}_1/P_0$ and Becker to the stabilised Q_1/Q_1 element [3, 12, 15, 32]. In all cases, the smoother is extensively tested on the benchmark configuration 'Flow around a cylinder' [33] for the steady and unsteady state. Ouazzi and Turek [22] transfer the Vanka idea to edge-oriented storage- and stabilisation techniques for Navier-Stokes equations. Zeng and Wesseling [38] compare Vanka-type smoothers to ILU methods for the case of Navier-Stokes in general coordinates. To treat anisotropic grids more robustly, several extensions have been introduced. Thompson and Ferziger define *symmetrically coupled alternating line (SCAL)* versions for Finite Difference discretisations, Becker uses a *string-wise* version for the stabilised Q_1/Q_1 discretisation, and Schmachtel develops an adaptive blocking strategy [3, 28, 31]. John and Matthies successfully apply Vanka smoothers to higher order finite element methods [13, 14]. Comparative solver studies including Vanka smoothers can be found in the articles of Benzi and Olshanskii [4] and Larin and Reusken [18].

There are only few papers describing the use of Vanka-type smoothers in the context of CSM. For many kinds of solid mechanical problems there is obviously no need to refrain from standard (point-wise) multigrid smoothers. But for special formula-

tions, which are used to treat (nearly) incompressible material effects, similar equation systems as for Navier-Stokes arise such that in this case the use of Vanka-type smoothers makes sense. Suttmeier [30] applies the variant developed by Becker [3] to elasto-plastic materials and compares it to standard Gauß-Seidel smoothing. Gaspar et al. [9] compare Vanka-type smoothers to decoupled smoothers in the context of incompressible poroelasticity equations. Hron and Turek [11] employ Vanka smoothers to solve coupled systems arising from the Q_2/P_1 discretisation of Fluid Structure Interaction problems.

The aim of this paper is to further close this gap by presenting extensive numerical studies of Vanka-type smoothers applied to CSM problems. The scope of the paper is described by the following aspects:

- Hyperelastic material behaviour (linear and nonlinear) is considered.
- Stationary computations are performed.
- As discretisation techniques pure displacement and mixed formulations with (conforming) Q_1 and stabilised Q_1/Q_1, respectively, are applied.
- For the (geometric) multigrid algorithm only 'standard' components are used (e. g., no adaptive step-length control [12] or matrix-dependent grid transfer).
- Only the 'standard' block Gauß-Seidel iteration is applied, lining- or adaptive patching-strategies as mentioned above are not considered.
- Four variants of Vanka-type smoothers are examined. A comparison to other smoother classes like global (decoupled) Schur complement smoothers [32] is beyond the scope of this paper and will be part of our future work.

The paper is organised as follows: In Section 2 the underlying partial differential equations and their discretisations are described. In Section 3 different Vanka-type smoothers are introduced and numerically investigated in the main Section 4. The last section presents a summarising evaluation.

2 Elasticity equations

2.1 Linear elasticity

We consider a solid body $\bar{\Omega} \subset \mathbb{R}^d$ ($d = 2, 3$) with Ω being a bounded, open set with boundary $\Gamma := \partial\Omega$. The boundary is split into the Dirichlet part Γ_D where displacements are presribed and the Neumann part Γ_N where traction forces can be applied ($\Gamma_\mathrm{D} \cap \Gamma_\mathrm{N} = \emptyset$). Furthermore the body can be exposed to volumetric forces like gravity. The current state of the body is described by a mapping $\boldsymbol{\Phi} : \bar{\Omega} \to \mathbb{R}^d$, called *deformation* in the case of $\det(\nabla\boldsymbol{\Phi}) > 0$. It can be written as $\boldsymbol{\Phi} = \mathbf{id} + \boldsymbol{u}$, where $\boldsymbol{u}(\boldsymbol{x}) = \big(u_1(\boldsymbol{x}), \dots, u_d(\boldsymbol{x})\big)^\mathsf{T}$ is the displacement of a material point $\boldsymbol{x} \in \bar{\Omega}$. Assuming only *small deformations* the kinematic relation between displacements and strains can be described with the linearised strain tensor

$$\boldsymbol{\varepsilon} = \frac{1}{2}(\nabla\boldsymbol{u} + \nabla\boldsymbol{u}^\mathsf{T}). \tag{2.1}$$

The response of a body to an external load depends on the material the body consists of. The material properties are reflected by the relation between the strains and the stresses, the *constitutive law*. If the stresses only depend on the current strains (and not on the history of strains and stresses) the material behaviour is called *elastic*. If, additionally, for the displacements only terms of first order are considered and the material is isotropic, we end up with the *linear material law of Hooke*:

$$\boldsymbol{\sigma} = 2\mu\boldsymbol{\varepsilon} + \lambda\,\mathrm{tr}(\boldsymbol{\varepsilon})\boldsymbol{I}. \tag{2.2}$$

Here, $\boldsymbol{\sigma}$ is the symmetric Cauchy stress tensor which depends linearly on the strain tensor $\boldsymbol{\varepsilon}$. μ and λ are the *Lamé constants* which are connected to *Young's modulus* E and the *Poisson ratio* ν via

$$\mu = \frac{E}{2(1+\nu)} \quad \text{and} \quad \lambda = \frac{E\nu}{(1+\nu)(1-2\nu)}.$$

The basic physical equation for problems of solid mechanics is given by the *equilibrium conditions*: for a body in equilibrium, the inner forces (stresses) and the outer forces (external loads) are balanced, i. e.

$$-\operatorname{div}\boldsymbol{\sigma} = \boldsymbol{f}, \qquad \text{in } \Omega. \tag{2.3}$$

(Inertial forces are not considered here.) Using Hooke's law (2.2) to substitute the stress tensor, the problem of linear elasticity can be expressed in terms of the following elliptic boundary value problem, called the *Lamé equation*:

$$\begin{aligned} -2\mu\,\operatorname{div}\boldsymbol{\varepsilon} - \lambda\,\operatorname{grad}\operatorname{div}\boldsymbol{u} &= \boldsymbol{f}, & \boldsymbol{x} &\in \Omega, \\ \boldsymbol{u} &= \boldsymbol{0}, & \boldsymbol{x} &\in \Gamma_{\mathrm{D}}, \\ \boldsymbol{\sigma}\boldsymbol{n} &= \boldsymbol{t}, & \boldsymbol{x} &\in \Gamma_{\mathrm{N}}. \end{aligned}$$

To simplify notation we consider only zero boundary conditions on Γ_{D}; $\boldsymbol{t}$ denotes given traction forces on Γ_{N} with outer normal $\boldsymbol{n}$. The only unknowns are the displacements $\boldsymbol{u}$, while strains and the stresses can be computed via relations (2.1) and (2.2).

Defining the space $\boldsymbol{X} := \left\{\boldsymbol{v} \in H^1(\Omega)^d \;\middle|\; \boldsymbol{v}\big|_{\Gamma_{\mathrm{D}}} = \boldsymbol{0}\right\}$ and the products

$$\begin{aligned} \boldsymbol{\varepsilon}(\boldsymbol{u}) : \boldsymbol{\varepsilon}(\boldsymbol{v}) &:= \sum_{i,j=1}^{d} \varepsilon_{ij}(\boldsymbol{u})\varepsilon_{ij}(\boldsymbol{v}), & (\boldsymbol{f},\boldsymbol{v})_0 &:= \int_\Omega \boldsymbol{f}\cdot\boldsymbol{v}\,\mathrm{d}v, \\ \big(\boldsymbol{\varepsilon}(\boldsymbol{u}),\boldsymbol{\varepsilon}(\boldsymbol{v})\big)_0 &:= \int_\Omega \boldsymbol{\varepsilon}(\boldsymbol{u}) : \boldsymbol{\varepsilon}(\boldsymbol{v})\,\mathrm{d}v, & (\boldsymbol{t},\boldsymbol{v})_\Gamma &:= \int_{\Gamma_{\mathrm{N}}} \boldsymbol{t}\cdot\boldsymbol{v}\,da, \end{aligned}$$

the weak formulation reads: Find $\boldsymbol{u} \in \boldsymbol{X}$ such that

$$2\mu\big(\boldsymbol{\varepsilon}(\boldsymbol{u}),\boldsymbol{\varepsilon}(\boldsymbol{v})\big)_0 + \lambda(\operatorname{div}\boldsymbol{u},\operatorname{div}\boldsymbol{v})_0 = (\boldsymbol{f},\boldsymbol{v})_0 + (\boldsymbol{t},\boldsymbol{v})_\Gamma, \qquad \boldsymbol{v} \in \boldsymbol{X}. \tag{2.4}$$

To transform the continuous problem (2.4) into a discrete one, the domain $\bar{\Omega}$ is approximated by a domain $\bar{\Omega}^h$. In our case, $\bar{\Omega}^h$ consists of m non-overlapping patches

$\bar{\Omega}_i^h$, i. e. $\bar{\Omega}^h = \cup_{i=1}^m \bar{\Omega}_i^h$. Each patch itself is a *generalised tensor product mesh*, i. e. inner patch nodes have exactly four neighbouring nodes. The superscript h symbolically denotes the refinement level of the grid. The approximate solution $\boldsymbol{u}^h$ of equation (2.4) is sought within a finite dimensional subspace $\boldsymbol{X}^h \subset \boldsymbol{X}$ which is defined by nodal basis functions $\phi_i, i = 1, \ldots, n$, with $n = \dim(\boldsymbol{X}^h)/d$. We use the standard bilinear element Q_1, so n coincides with the number of mesh vertices not lying on Γ_D. Consequently, the discrete analogon to equation (2.4) is: Find $\boldsymbol{u}^h \in \boldsymbol{X}^h$ such that

$$2\mu\big(\boldsymbol{\varepsilon}(\boldsymbol{u}^h), \boldsymbol{\varepsilon}(\boldsymbol{v})\big)_0 + \lambda(\operatorname{div}\boldsymbol{u}^h, \operatorname{div}\boldsymbol{v})_0 = (\boldsymbol{f}, \boldsymbol{v})_0 + (\boldsymbol{t}, \boldsymbol{v})_\Gamma, \qquad \boldsymbol{v} \in \boldsymbol{X}^h, \tag{2.5}$$

where the integrals are now evaluated over Ω^h.

Based on equation (2.5) the linear system of equations $\mathbf{K}\mathbf{u} = \mathbf{f}$ is assembled in the usual manner. Here, $\mathbf{u} = (\mathbf{u}_1, \ldots, \mathbf{u}_d)^\mathsf{T} \in \mathbb{R}^{dn}$ is the unknown coefficient vector with $u_j^h = \sum_{i=1}^n (\mathbf{u}_j)_i \phi_i, j = 1, \ldots, d$, while $\mathbf{K} \in \mathbb{R}^{dn \times dn}$ and $\mathbf{f} \in \mathbb{R}^{dn}$ are the stiffness matrix and the discrete external load vector. Note, that throughout the paper bold upright letters are used to describe discrete vectors $\mathbf{v} \in \mathbb{R}^l$ and matrices $\mathbf{M} \in \mathbb{R}^{l \times l}$, $l \in \mathbb{N}$.

2.2 Nearly incompressible material

It is well known that the above formulation (2.5) fails for *nearly incompressible* materials (e. g. rubber) for which the Poisson ratio ν is close to 0.5 and the Lamé constant λ tends to infinity. When applying formulation (2.5) for such materials two severe problems arise: First, iterative solving schemes deteriorate due to a high condition number of the resulting system matrix. Second, the approximation error of the finite element scheme (2.5) increases, a phenomenon widely known as *volume locking* (see [1,2,7]). To overcome these deficiencies we translate the above *pure displacement formulation* (2.5) into a *mixed formulation*. The idea is to treat the critical parameter λ by introducing a new variable

$$p := -\lambda \operatorname{div}\boldsymbol{u},$$

which can be interpreted as *pressure*. The Lamé equation thus turns into the following mixed problem:

$$\begin{aligned} -2\mu \operatorname{div}\boldsymbol{\varepsilon} + \nabla p &= \boldsymbol{f}, && \boldsymbol{x} \in \Omega, \\ -\operatorname{div}\boldsymbol{u} - \lambda^{-1} p &= 0, && \boldsymbol{x} \in \Omega, \\ \boldsymbol{u} &= \boldsymbol{0}, && \boldsymbol{x} \in \Gamma_\mathrm{D}, \\ \boldsymbol{\sigma}\boldsymbol{n} &= \boldsymbol{t}, && \boldsymbol{x} \in \Gamma_\mathrm{N}. \end{aligned} \tag{2.6}$$

This means, the critical 'large' parameter λ has turned into the 'small' one λ^{-1} with $\lambda^{-1} \to 0$ for $\nu \to 0.5$. With $M := L_2(\Omega)$ being the pressure space the weak formulation of (2.6) reads: Find $(\boldsymbol{u}, p) \in \boldsymbol{X} \times M$, such that

$$2\mu\big(\boldsymbol{\varepsilon}(\boldsymbol{u}), \boldsymbol{\varepsilon}(\boldsymbol{v})\big)_0 - (\operatorname{div}\boldsymbol{v}, p)_0 = (\boldsymbol{f}, \boldsymbol{v})_0 + (\boldsymbol{t}, \boldsymbol{v})_\Gamma, \qquad \boldsymbol{v} \in \boldsymbol{X}, \tag{2.7a}$$

$$-(\operatorname{div}\boldsymbol{u}, q)_0 - \lambda^{-1}(p, q)_0 = 0, \qquad q \in M. \tag{2.7b}$$

In terms of the three continuous bilinear forms

$$\begin{aligned} a(\cdot,\cdot) &: \boldsymbol{X} \times \boldsymbol{X} \to \mathbb{R}, \qquad a(\boldsymbol{u},\boldsymbol{v}) := 2\mu\big(\boldsymbol{\varepsilon}(\boldsymbol{u}),\boldsymbol{\varepsilon}(\boldsymbol{v})\big)_0, \\ b(\cdot,\cdot) &: \boldsymbol{X} \times M \to \mathbb{R}, \qquad b(\boldsymbol{v},p) := -(\operatorname{div}\boldsymbol{v},p)_0, \\ c(\cdot,\cdot) &: M \times M \to \mathbb{R}, \qquad c(p,q) := (p,q)_0, \end{aligned}$$

the weak formulation (2.7) can be rewritten as

$$\begin{aligned} a(\boldsymbol{u},\boldsymbol{v}) + b(\boldsymbol{v},p) &= (\boldsymbol{f},\boldsymbol{v})_0 + (\boldsymbol{t},\boldsymbol{v})_\Gamma, \qquad && \boldsymbol{v} \in \boldsymbol{X}, \\ b(\boldsymbol{u},q) - \lambda^{-1} c(p,q) &= 0, && q \in M, \end{aligned}$$

revealing the structure of a saddle point problem with a penalty term, namely λ^{-1}. Equation (2.7) has a unique solution when the well known *LBB conditions* are fulfilled [7]:

1. The continuous bilinear form $a(\cdot,\cdot)$ is $\boldsymbol{X}$-elliptic;
2. For the continuous bilinear form $b(\cdot,\cdot)$ the *inf-sup condition* holds:

$$\exists\, \beta > 0 : \quad \inf_{q \in M} \sup_{\boldsymbol{v} \in \boldsymbol{X}} \frac{b(\boldsymbol{v},q)}{\|\boldsymbol{v}\|_1 \, \|q\|_0} \geqslant \beta.$$

Here, $\|\cdot\|_1$ and $\|\cdot\|_0$ are the usual norms induced by the scalar products of the spaces $H^1(\Omega)^d$ and $L_2(\Omega)$, resp. When discretising the problem, one has to pay attention to the choice of the corresponding finite element spaces $\boldsymbol{X}^h$ and M^h. If they fulfill a discrete analogon of the LBB conditions, the finite element approximation converges robustly, i. e. independent of the parameter λ, to the real solution. It is known that element pairs which are suitable for the Stokes equation can also be employed for discretising equation (2.7).

The problem of finding efficient finite element pairs for the Stokes equation has been studied intensively. Since the LBB condition is rather restrictive, many element combinations drop out. For example, equal order element pairs, which are attractive from an implementational point of view, are known to be unstable (e. g., Q_1/Q_1). Hence, many strategies were developed to *stabilise* such element combinations. Bochev et al. [5] provide an overview and a classification. We use an extension of the method introduced by Becker [3], which is robust even on highly anisotropic grids. The stabilisation terms can be expressed with help of the bilinear form (assume $d = 2$ for illustration):

$$c_{s,h}(p,q) := \frac{\alpha}{2\mu} \sum_e \int_{\Omega_e^h} \boldsymbol{\xi}_e{}^{\mathsf{T}} \nabla p \; \boldsymbol{\xi}_e{}^{\mathsf{T}} \nabla q + \boldsymbol{\eta}_e{}^{\mathsf{T}} \nabla p \; \boldsymbol{\eta}_e{}^{\mathsf{T}} \nabla q \; \mathrm{d}v. \tag{2.8}$$

Here, e loops over all elements Ω_e^h of Ω^h, $\boldsymbol{\xi}_e$ and $\boldsymbol{\eta}_e$ describe the local coordinate system of the element e (see Fig. 1), and α is a stabilisation parameter which is set to $\alpha = 0.1$ throughout the paper. In case of a cartesian grid (where $\boldsymbol{\xi}$ and $\boldsymbol{\eta}$ are parallel to x-

and y-axis, resp.) stabilisation (2.8) coincides with that of Becker [3]. As in the pure displacement formulation, we end up with a linear system of equations

$$\begin{pmatrix} \mathbf{A} & \mathbf{B} \\ \mathbf{B}^{\mathsf{T}} & \mathbf{C} \end{pmatrix} \begin{pmatrix} \mathbf{u} \\ \mathbf{p} \end{pmatrix} = \begin{pmatrix} \mathbf{f} \\ \mathbf{g} \end{pmatrix}, \tag{2.9}$$

where the matrix $\mathbf{C}$ contains the compressibility terms (2.7b) and the stabilisation terms (2.8).

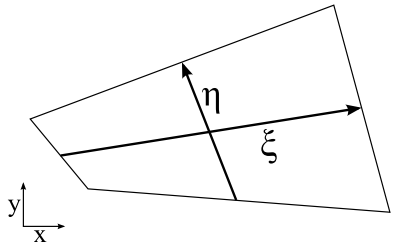

Figure 1: Local coordinate system of an element.

2.3 Finite elasticity

In many applications the assumption of *small* deformations is not realistic and has to be dropped [19]. To formulate the balance equation with respect to the reference configuration the *first Piola-Kirchhoff stress tensor* $\boldsymbol{P}$ can be used. It is connected to the Cauchy stress tensor $\boldsymbol{\sigma}$ via the relation $\boldsymbol{P} := J\boldsymbol{\sigma}\boldsymbol{F}^{-\mathsf{T}}$ where $\boldsymbol{F} := \boldsymbol{I} + \nabla\boldsymbol{u}$ is the *deformation gradient* and $J := \det(\boldsymbol{F})$. The resulting boundary value problem then reads

$$\begin{aligned} -\operatorname{div}\boldsymbol{P} &= \boldsymbol{f}, & \boldsymbol{x} &\in \Omega, \\ \boldsymbol{u} &= \boldsymbol{0}, & \boldsymbol{x} &\in \Gamma_{\mathrm{D}}, \\ \boldsymbol{P}\boldsymbol{n} &= \boldsymbol{t}, & \boldsymbol{x} &\in \Gamma_{\mathrm{N}}. \end{aligned}$$

The corresponding weak formulation is

$$(\boldsymbol{P}, \nabla\boldsymbol{v})_0 = (\boldsymbol{f}, \boldsymbol{v})_0 + (\boldsymbol{t}, \boldsymbol{v})_\Gamma, \quad \boldsymbol{v} \in \boldsymbol{X}, \tag{2.10}$$

where again the above definition $(\boldsymbol{P}, \nabla\boldsymbol{v})_0 := \int_\Omega \boldsymbol{P} : \nabla\boldsymbol{v}\,\mathrm{d}v$ is used. In the context of this paper we employ the constitutive law of hyperelastic Neo-Hooke material, which in terms of the first Piola-Kirchhoff stress tensor has the form

$$\boldsymbol{P} = \mu(\boldsymbol{F} - \boldsymbol{F}^{-\mathsf{T}}) + \frac{\lambda}{2}(J^2 - 1)\boldsymbol{F}^{-\mathsf{T}}. \tag{2.11}$$

With help of the residual vector $\mathbf{r}(\mathbf{u})$ measuring the imbalance of inner and outer forces the discrete analogon of equation (2.10) can be expressed in compact form $\mathbf{r}(\mathbf{u}) = 0$. We now face two kinds of *nonlinearity*. On the one hand there is the *geometric nonlinearity* resulting from the nonlinear kinematic relation between displacements and strains. On the other hand, the constitutive law (2.11) shows a nonlinear dependence of the stress tensor $\boldsymbol{P}$ on the deformation gradient $\boldsymbol{F}$, called *material*

or *physical nonlinearity*. Hence, a nonlinear solving mechanism is necessary to solve equation (2.10). We use a standard *Newton-Raphson scheme*

$$\mathbf{r}(\mathbf{u}^k) + \frac{\partial \mathbf{r}(\mathbf{u}^k)}{\partial \mathbf{u}}(\mathbf{u}^{k+1} - \mathbf{u}^k) = 0,$$

where $\mathbf{K}(\mathbf{u}^k) := \partial \mathbf{r}(\mathbf{u}^k)/\partial \mathbf{u}$ is the Jacobi matrix and $\Delta \mathbf{u}^{k+1} := \mathbf{u}^k - \mathbf{u}^{k+1}$ the update for the solution vector. So, in every Newton-Raphson iteration a linear system of the following form has to be solved:

$$\mathbf{K}(\mathbf{u}^k)\Delta \mathbf{u}^{k+1} = \mathbf{r}(\mathbf{u}^k).$$

Incompressible material in the finite elasticity setting is characterised by the deformation gradient's determinant J being close to 1. (Actually, the condition $\operatorname{div} \boldsymbol{u} = 0$ in the case of small deformation is nothing else then the linearised form of the condition $\det(\boldsymbol{F}) = 1$.) As in the linear case the arising critical term $\lambda(J^2 - 1)/2$ in the constitutive relation (2.11) is treated by introducing the pressure variable $p := -\lambda(J^2 - 1)/2$, such that the first Piola-Kirchhoff stress tensor takes the form $\boldsymbol{P} = \mu(\boldsymbol{F} - \boldsymbol{F}^{-\mathsf{T}}) - p\boldsymbol{F}^{-\mathsf{T}}$. Analogous to the pure displacement case we solve the resulting discrete residual equation $\mathbf{r}(\mathbf{u}, \mathbf{p}) = 0$ with help of a Newton-Raphson scheme

$$\mathbf{r}(\mathbf{u}^k, \mathbf{p}^k) + \frac{\partial \mathbf{r}(\mathbf{u}^k, \mathbf{p}^k)}{\partial (\mathbf{u}, \mathbf{p})} \left[\begin{pmatrix} \mathbf{u}^{k+1} \\ \mathbf{p}^{k+1} \end{pmatrix} - \begin{pmatrix} \mathbf{u}^k \\ \mathbf{p}^k \end{pmatrix} \right] = 0.$$

The linear systems arising in each Newton-Raphson step have a similar saddle point structure as in the small deformation setting, namely

$$\begin{pmatrix} \mathbf{A} & \mathbf{B} \\ \mathbf{D} & \mathbf{C} \end{pmatrix} \begin{pmatrix} \Delta \mathbf{u}^{k+1} \\ \Delta \mathbf{p}^{k+1} \end{pmatrix} = \mathbf{r}(\mathbf{u}^k, \mathbf{p}^k).$$

Depending on the constitutive law, we might have $\mathbf{D} \neq \mathbf{B}^{\mathsf{T}}$, resulting in an unsymmetric system matrix.

Remark: For sake of simplicity we will from now on consider the two-dimensional plane strain model only ($d = 2$): The body is assumed to be long in x_3-direction while load and geometry do not vary along this direction. Thus, it is justified to look at a cross section in the (x_1, x_2)-plane. Applied forces must have zero x_3-components, and only displacements in x_1- and x_2-direction need to be considered. The concepts described in the following sections can be transferred to the three-dimensional case without any complications.

3 Vanka-type smoothers

A geometric multigrid solver is mainly characterised by three components, namely the smoother, the grid transfer and the coarse grid solver. For the latter two we use

standard operations, i. e. inclusion for prolongation, the adjoint operation for restriction and a direct solver to treat the coarse grid problems. For a general introduction to multigrid we refer to the book of Hackbusch [10].

The robustness of the multigrid algorithm mainly depends on the smoothing procedure. We compare four variants of Vanka-type smoothers whose basic common idea is to decompose the mesh into small subdomains and treat these subdomains separately. In more detail, one smoothing step consists of a loop over all subdomains where in each iteration the following steps are performed:

1. *Extract the entries of the global matrix corresponding to the degrees of freedom (DOFs) of the current subdomain and assemble them into a small local matrix.*
2. *Build the corresponding local residual.*
   This is done in a Gauß-Seidel manner, i. e. information, which has been updated in previously treated subdomains, is immediately incorporated into the assembly process of the current local residual.
3. *Solve the resulting system with the local residual as right hand side.*
   Note, that the resulting local matrices are always invertible: When the subdomain lies in the interior of the mesh the local matrix contains the 'full' entries of the global matrix and can therefore be interpreted as arising from a mesh consisting of the subdomain itself enclosed by a further element layer with zero Dirichlet boundary conditions. When the subdomain lies at the boundary, the local system 'inherits' the boundary information of the global matrix, i. e. unit rows/columns in case of Dirichlet boundary and 'half' entries in case of Neumann boundary, respectively. We employ direct solvers (e. g. LAPACK) to invert the systems.
4. *Update the corresponding parts of the global solution with this local correction.*

The four Vanka variants differ in the choice of the subdomains and how the local systems are built.

Remark: As mentioned in Section 2.1, the domain $\bar{\Omega}^h$ consists of one or more tensor product patches $\bar{\Omega}_i^h$. In the smoothing process these patches are treated consecutively. Within one patch the small subdomains are traversed rowwise from the 'lower left' to the 'upper right' corner.

The cell-based Vanka smoother

The first variant to be described is the *cell-based* Vanka smoother. Here, each subdomain consists of exactly one element and the local system matrix contains the DOFs of the four element nodes (see Fig. 2, left). The smoother can be seen as a multiplicative domain decomposition method with *minimal overlap*, i. e. the subdomains (=elements) only intersect at their (element) boundaries. This minimises computational overhead.

Let e be the current element in the smoothing procedure, let the restriction of a vector or a matrix to this element be denoted with the index e, and let ω be a relaxation

parameter. Then the necessary calculations can be formulated as follows:

$$\begin{aligned} &\text{local residual} && \mathbf{r}_{\text{loc}} = \mathbf{f}_e - (\mathbf{K}\mathbf{u})_e, \\ &\text{local correction} && \mathbf{x}_{\text{loc}} = \mathbf{K}_e^{-1}\mathbf{r}_{\text{loc}}, \\ &\text{update of global solution} && \mathbf{u}_e = \mathbf{u}_e + \omega\mathbf{x}_e. \end{aligned} \tag{3.1}$$

The advantage of this smoother variant is that, without any changes, it can be applied directly to the saddle point system (2.9) arising from the mixed formulation. The additional matrix blocks $\mathbf{B}, \mathbf{B}^{\mathsf{T}}$ and $\mathbf{C}$ are automatically taken into account by simply incorporating the pressure as additional DOF, i. e. displacements and pressure are treated equally (see Fig. 2, left). This makes the smoother very attractive from an implementational point of view as it can be applied to arbitrarily coupled equation systems without deeper knowledge about the underlying problem. It clearly distinguishes this Q_1/Q_1 variant of the Vanka smoother from the original version of [35] where the pressure is represented in the local system with only one DOF.

Remark: The local relaxation with the parameter ω is different from global damping in the multigrid method: The local residuals corresponding to the subsequently treated elements are immediately affected by the relaxation, whereas the damping in the multigrid method scales the global correction vector *after* completion of the smoothing procedure. We emphasise this since a popular strategy for improving multigrid is to enclose the smoother by some Krylov space method [17]. The benefit of doing so is the 'automatic choice' of the correct damping parameter such that the multigrid's robustness is considerably increased. The (locally acting) relaxation parameter, however, can *not* be 'adjusted' this way and is set manually by the user.

Remark: The vector $(\mathbf{K}\mathbf{u})_e$ can be computed in $\mathcal{O}(1)$ time due to the sparse structure of $\mathbf{K}$. (In case of 2D pure displacement formulation on a tensor-product mesh there are at most 18 non-zero elements per matrix row.)

The patch-based Vanka smoother

In [3] the standard Vanka smoother is adapted for the stabilised Q_1/Q_1-discretisation and used for solving the incompressible Navier-Stokes equations. Due to the similar structure of the linear equation systems arising in this context, the adapted smoother can be applied to the mixed formulation in CSM, as well. This has been done, for instance, in [30] for the case of elasto-plastic material.

Instead of looping over all elements in the mesh we iterate over all pressure DOFs, i. e. over all nodes of the mesh. For each of them the displacements coupling with the node are taken into account such that in case of a tensor product mesh a patch consisting of the four adjacent elements has to be considered (see Fig. 2, center).

The corresponding local systems to be solved have the following form then:

$$\begin{pmatrix} a_{11} & \dots & a_{1n} & b_1 \\ \vdots & \ddots & \vdots & \vdots \\ a_{n1} & \dots & a_{nn} & b_n \\ d_1 & \dots & d_n & c \end{pmatrix} \begin{pmatrix} x_1 \\ \vdots \\ x_n \\ y \end{pmatrix} = \begin{pmatrix} f_1 \\ \vdots \\ f_n \\ f \end{pmatrix}.$$

In case of 2D and the patch center being an inner mesh node we have $n = 18$. For linear elasticity $d_i = b_i, i = 1, \ldots, n$, holds.

The motivation behind this approach is that in case of Q_1-discretisation the incompressibility constraint $\operatorname{div} \boldsymbol{u} = 0$ can, in general, not be met locally in *one* element. It *is* possible, however, to fulfill this condition locally by increasing the number of involved displacement DOFs, e. g. by considering the whole patch around one node. Moreover, the ratio between number of displacement and pressure DOFs better reflects the fact that in (2.6) the order of displacement derivatives is higher than the order of pressure derivatives, i. e. displacements should be approximated 'more accurately'.

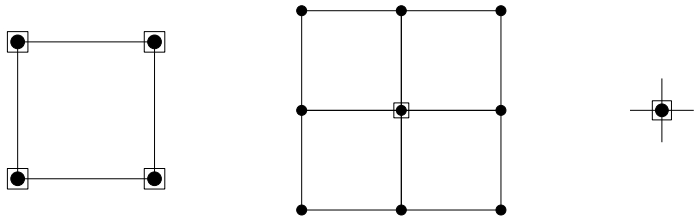

Figure 2: Subdomains for cell-, patch- and vertex-based Vanka smoother and the corresponding DOFs. (• displacement DOFs, □ pressure DOFs)

So, the patch-based Vanka smoother should be better suited for (nearly) incompressible material behaviour, which will be confirmed numerically in Section 4. There, we also examine whether simulations with compressible material also benefit from this smoother modification.

Compared to the cell-based Vanka smoother described in the previous section the patch-based variant has some disadvantages, where the last one is only a minor implementational issue.

- The resulting local systems are larger such that more time for the LU decomposition is needed.
- The patches overlap each other by one element layer which means some more computational overhead.
- With its special form (taking the third DOF only in the patch center) the patch-based variant is only applicable to the mixed $\boldsymbol{u}/p$ formulation, but not to the pure displacement case. (The idea of overlapping patches, however, *could* be transferred to the pure displacement case, of course. But this is not done in this paper.)
- Assembling the local systems is more involved since a larger neighbourhood has to be considered.

In Section 4 we will see in terms of iteration numbers and total computation times if the numerical benefits of the patch-based approach outweigh these disadvantages.

The patch-based diagonal Vanka smoother

Becker [3] and Suttmeier [30] apply a simplified variant of the patch-based Vanka smoother. The idea is to couple each displacement DOF only with itself such that the upper left $n \times n$-part of the local matrix is a diagonal matrix:

$$\begin{pmatrix} a_{11} & 0 & \dots & 0 & b_1 \\ 0 & a_{22} & \ddots & \vdots & \vdots \\ \vdots & \ddots & \ddots & 0 & \vdots \\ 0 & \dots & 0 & a_{nn} & b_n \\ d_1 & \dots & \dots & d_n & c \end{pmatrix} \begin{pmatrix} x_1 \\ \vdots \\ \vdots \\ x_n \\ y \end{pmatrix} = \begin{pmatrix} f_1 \\ \vdots \\ \vdots \\ f_n \\ f \end{pmatrix}.$$

Denoting this system with

$$\begin{pmatrix} \mathbf{D} & \mathbf{b} \\ \mathbf{d}^T & c \end{pmatrix} \begin{pmatrix} \mathbf{x} \\ y \end{pmatrix} = \begin{pmatrix} \mathbf{f} \\ f \end{pmatrix},$$

it can be solved very easily by eliminating $\mathbf{x}$:

$$y = \frac{\mathbf{d}^T\mathbf{D}^{-1}\mathbf{f} - f}{\mathbf{d}^T\mathbf{D}^{-1}\mathbf{b} - c}, \qquad \mathbf{x} = \mathbf{D}^{-1}(\mathbf{f} - y\mathbf{b}).$$

Basically, this can be performed with two scalar products and two vector-vector multplications/additions which is much cheaper than applying an LU decomposition to the whole $(n+1) \times (n+1)$-system as in the full patch-based approach.

It has been observed that diagonal variants of the Vanka smoother are less robust with respect to mesh anisotropies in the context of incompressible Navier-Stokes equations (e. g., [27]). In Section 4 we will examine this point for the elasticity case.

The vertex-based diagonal 'Vanka smoother'

For sake of completeness we consider an even simpler smoother variant where the 'subdomain' consists of only one vertex (see Fig. 2, right). Now we let each DOF only couple with itself, such that the system to be 'solved' looks, in case of 2D mixed formulation, as following:

$$\begin{pmatrix} a_{11} & 0 & 0 \\ 0 & a_{22} & 0 \\ 0 & 0 & c \end{pmatrix} \begin{pmatrix} x_1 \\ x_2 \\ y \end{pmatrix} = \begin{pmatrix} f_1 \\ f_2 \\ f \end{pmatrix}.$$

Actually, this describes the standard Gauß-Seidel smoother. But, according to the above constructions it could also be interpreted as *vertex-based diagonal Vanka smoother*. Thus, it can be seen as the first one in a Vanka smoothers' hierarchy which is determined by the size of the subdomains:

$$\text{vertex} \quad \rightarrow \quad \text{cell} \quad \rightarrow \quad \text{patch}.$$

(Of course, one could further investigate variants of the vertex-based Vanka smoother where the above local matrix is not diagonal, but this is not done here.)

4 Numerical studies

In this section the four Vanka smoothers are tested and compared with respect to the following aspects: mesh anisotropies, compressible and nearly incompressible material, small and finite deformation, relaxation parameter ω, number of pre- and postsmoothing steps τ.

4.1 Specifications

Usually we employ multigrid as stand-alone solver, but in some cases it is beneficial or even necessary to use multigrid as a preconditioner within an outer iterative method. In that case we use BICGSTAB [34] as outer solver and do exactly one multigrid step for preconditioning. Abbreviations for the employed solver components are as follows:

- MG-GS: multigrid with standard Gauß-Seidel smoother (at the end of Section 3 denoted as *vertex-based Vanka smoother*);
- MG-VANKA-C: multigrid with cell-based Vanka smoother;
- MG-VANKA-P: multigrid with patch-based Vanka smoother;
- MG-VANKA-PD: multigrid with patch-based Vanka smoother, diagonal displacement matrix;
- BICG-MG-VANKA-*: corresponding BICGSTAB solver with multigrid as preconditioner.

We always use the F-cycle with equal number τ of pre- and postsmoothing steps and a (global) damping parameter of 1.0.[†] The iteration is stopped either after 64 iterations (32 iterations for the BiCG-variants, 128 iterations for standard Gauß-Seidel smoother) or when the initial residual is reduced by a factor of 10^{-6}. If the solver did not converge within the 64 (32, 128) iterations, there are two possibilities: First, when the convergence rate is less than 1, then this is indicated by the entry '$>$ 64 '('$>$ 32','$>$ 128'), i. e. the solver probably would have converged after more iterations. Second, when the convergence rate is greater than 1, then this is indicated by the entry '-', i. e. the solver probably would have diverged after more iterations. Divergence within the maximal iteration number is also denoted by '-'. The last table row shows the linear solving times for the finest level computation. All simulations were performed on an AMD Opteron 250 with a CPU frequency of 2400 MHz and 7.6 GB main memory.

We define several prototypical configurations which are characterised by the mesh, the material parameters and the right hand side terms.

Configuration ANALYTIC: In this configuration the unit square with different degrees of mesh anisotropy is considered. The coarse grid is prerefined anisotropically towards the lower left corner such that element aspect ratios of 1,4 and 16, respectively, arise (see Fig. 3). The *aspect ratio* of an element is determined by measuring the

[†]We also tested other values for the damping parameter and found that its influence on the solver convergence - compared to that of the relaxation parameter - can be neglected.

distances between the midpoints of two opposing edges and then dividing the longer distance by the shorter one.

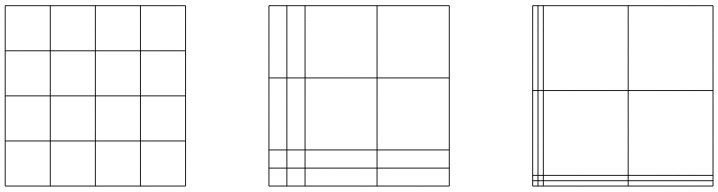

Figure 3: Coarse grids for the configuration ANALYTIC with element aspect ratios 1, 4, 16.

The further refinement for the multigrid algorithm is done in an isotropic way. The material parameters are $\mu = 0.5, \nu \in \{0.3, 0.5\}$. The prescribed right hand side terms are computed from given analytic solutions, which in case of $\nu = 0.3$ and $\nu = 0.5$, respectively, are

$$u_1(x,y) = x(1-x)y(1-y), \qquad u_1(x,y) = \sin(\pi x - 0.7)\sin(\pi y + 0.2),$$
$$u_2(x,y) = \frac{1}{20}\sin(4\pi x)\sin(4\pi y), \qquad u_2(x,y) = \cos(\pi x - 0.7)\cos(\pi y + 0.2),$$
$$p(x,y) = -\lambda \operatorname{div} \boldsymbol{u}(x,y), \qquad p(x,y) = \sin(x)\cos(y) + (\cos(1) - 1)\sin(1),$$

(taken from [30] and [6], resp.). On top, bottom and left side of the unit square domain Dirichlet boundary conditions for the displacements are prescribed, while we have Neumann boundary conditions corresponding to the analytical solution on the right side.

Configuration BEAM: This configuration describes a flexible beam which is fixed at its rounded left side (see Fig. 4(b)). The anisotropic version has a coarse grid of four elements with an element aspect ratio of 16 while the coarse grid of the 'isotropic' version consists of 32 elements with a maximal element aspect ratio of 3 (see Fig. 4(a)). The configuration stems from a Fluid-Structure-Interaction benchmark [11] where this flexible beam is attached to a cylinder and exposed to a fluid in a channel. The material constants are $\mu = 500000, \nu = 0.4999$, and the beam is loaded by a gravity force of $(0, -2000)$. What makes this pure structural part of the benchmark interesting is the fact that the body is thin and only a small portion of its boundary is fixed which is known to lead to numerical difficulties [7, 23].

Configuration CROSSOVER: This configuration is more like a 'real life' example. It describes the cross section of a rubber-like crossover which is used to slow down street traffic. Due to the two holes and the middle gap it has a rather complex geometry (see Fig. 5). The material constants are $\mu = 80.194, \nu = 0.4999$, and the surface load is only applied on the right half of the geometry. The standard version is isotropically refined, while in a second version the elements around the holes are *anisotropically refined* towards the holes to better resolve the arising stresses there (see Fig. 5(b)). This means, that the maximal element aspect ratio increases with the multigrid level (see Table 1).

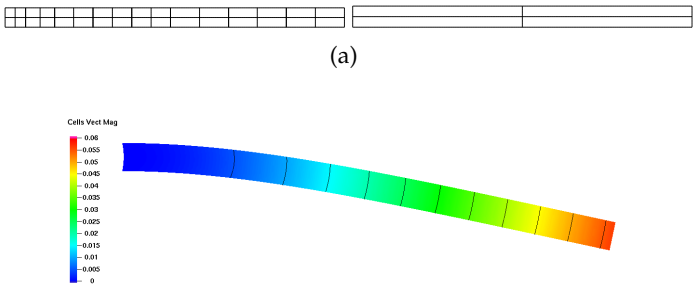

(a)

(b)

Figure 4: Configuration BEAM. (a) Coarse grids: iso and aniso, (b) deformed state ($\|\boldsymbol{u}\|$ displayed).

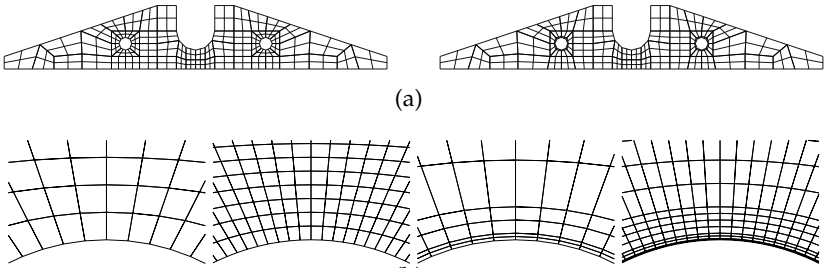

(a)

(b)

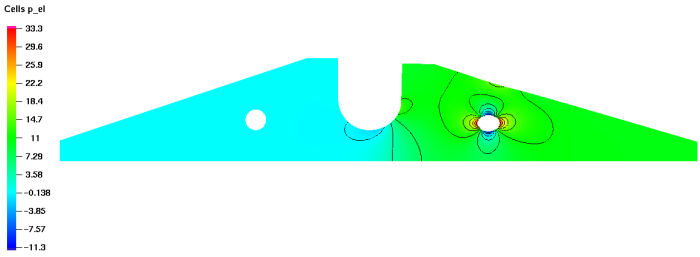

(c)

Figure 5: Configuration CROSSOVER. (a) Coarse grids: iso and aniso; (b) Magnified upper part of a hole: iso (level $3+4$) and aniso (level $3+4$); (c) Deformed state (pressure p displayed).

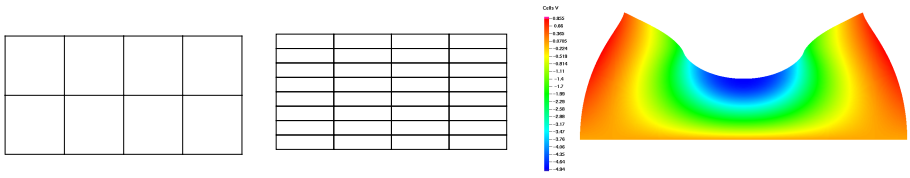

(a) (b)

Figure 6: Configuration BLOCK. (a) Coarse grids: iso and aniso, (b) Deformed state, load $(0,-300)$ (u_2 displayed).

Configuration BLOCK: A rectangular block is loaded by a surface force acting on the middle part of its top side (see Fig. 6). Reese et al. [26] employ this test to compare different Finite Element formulations for high compression rates in the context of finite deformation. Two different coarse meshes are used: BLOCK-ISO with 8 elements and aspect ratio 1, BLOCK-ANISO with 32 elements and aspect ratio 4 (see Fig. 6(a)). The material constants are $\mu = 80.194, \nu = 0.4999$, applied loads are $(0, t_y)$, $t_y \in \{-20, -300\}$.

In all configurations homogenous Neumann boundary conditions for the pressure are prescribed. Other parameters and information about the configurations are listed in Table 1.

Remark: The rather high aspect ratios of the configuration CROSSOVER-ANISO displayed in Table 1 only hold for the first two element layers enclosing the holes (see magnifications in Fig. 5(b)). So, the vast majority of the elements has comparatively mild aspect ratios. This distinguishes this configuration from the other anisotropic configurations where exactly half the elements (ANALYTIC) or all elements (BEAM, BLOCK) exhibit the listed high aspect ratios.

Remark: There is a vast number of possible combinations of configurations and parameters. So, to keep the amount of information manageable, we show in the following tables only those ranges of values which contain the optimal setting.

4.2 Compressible material

Pure displacement formulation

Vanka-type smoothers were originally developed for saddle point systems with a zero block on the diagonal. The systems stemming from the pure displacement formulation in elasticity do *not* belong to this class but are much simpler to treat due to their positive definiteness. Nevertheless, we want to test if it pays off to apply the Vanka idea to such systems as well. Therefore, we compare the cell-based Vanka and the standard (vertex-based) Gauß-Seidel smoother. As test environment we choose at first the configuration ANALYTIC with $\nu = 0.3$. Table 2(a) clearly shows that it does *not* pay off to use Vanka smoothing for this configuration. Though it needs less iterations than Gauß-Seidel smoothing, it is slower in terms of total computation time. Especially the slightly overrelaxed Gauß-Seidel smoother outperforms the Vanka smoother on more

Table 1: Number of elements on highest level, number m of patches, maximal element aspect ratios (AR), loads and material parameters of the test configurations. (Note the level-dependent aspect ratios of the CROSSOVER-ANISO configuration.)

Configuration	# el	m	max. AR	load	μ	ν
ANALYTIC1/4/16	262144	1	1 / 4 / 16	analytic	0.5	0.3, 0.5
BEAM-ISO	131072	8	3	$(0, -2000)$ (vol)	500000	0.4999
BEAM-ANISO	65536	1	16			
CROSSOVER-ISO	63488	62	3.1	$(0, -20)$	80.194	0.4999
CROSSOVER-ANISO			8.6 / 20.6 / 51.2 (lv 3/4/5)			
BLOCK-ISO	131072	8	1	$(0, -20), (0, -300)$	80.194	0.4999
BLOCK-ANISO		32	4			

Table 2: MG-GS vs. MG-VANKA-C; pure displacement formulation; $\nu = 0.3$. (a) ANALYTIC with aspect ratios 1, 4 and 16. (b) CROSSOVER-ISO/ANISO.

(a)

	MG-GS						MG-VANKA-C					
ω	0.8		1.0		1.2		0.8		1.0		1.2	
AR 1												
τ	1	2	1	2	1	2	1	2	1	2	1	2
lv 6	12	7	9	5	12	7	5	4	5	4	5	4
lv 7	12	7	9	5	13	7	5	4	5	4	5	4
lv 8	12	7	9	5	13	7	5	4	5	4	5	4
sec	23	26	17	18	25	25	48	76	47	77	48	78
AR 4												
τ	2	4	2	4	2	4	1	2	1	2	1	2
lv 6	57	28	41	20	29	14	23	12	22	11	22	12
lv 7	57	28	41	20	30	15	22	12	21	12	21	12
lv 8	56	28	40	20	30	14	22	13	21	12	22	13
sec	207	204	147	160	112	99	215	248	201	237	212	248
AR 16												
τ	16	32	16	32	16	32	4	8	4	8	4	8
lv 6	67	33	48	24	35	17	52	25	48	24	49	24
lv 7	79	39	57	28	42	21	57	28	53	26	53	26
lv 8	82	41	59	30	44	22	55	27	50	25	51	26
sec	2337	2378	1802	1715	1224	1240	2278	2086	1867	1925	2027	2043

(b)

	MG-GS				MG-VANKA-C			
ω	1.0		1.2		1.0		1.2	
iso								
τ	1	2	1	2	1	2	1	2
lv 3	23	13	18	11	10	6	10	6
lv 4	23	13	18	11	10	7	10	6
lv 5	22	13	17	11	9	6	10	6
sec	16	17	12	16	23	31	26	30
aniso								
τ	4	8	4	8	2	4	2	4
lv 3	12	8	10	7	8	6	8	6
lv 4	35	18	24	13	13	7	12	6
lv 5	90	45	63	32	28	15	28	14
sec	227	222	160	159	143	146	141	143

anisotropic meshes. On the other hand, one can state that the Vanka smoother is not as sensitive with respect to the relaxation parameter which can be seen as advantage.

As second test we consider the configuration CROSSOVER. In Table 2(b) one can see that for the isotropic case the smoothers show a similar behaviour as in the first test, but for the anisotropic case the Vanka smoother actually beats the Gauß-Seidel smoother.

Mixed formulation

Suttmeier [30] states that in the case of linear elasticity with compressible material the mixed formulation – although not necessary – can lead to better displacement approximations. So, it is reasonable to compare the two above smoothers also for this setting. The results for the configuration ANALYTIC are similar to the pure displacement case (compare Table 2(a) with Table 3(a)).

The crucial difference is that here overrelaxation of Gauß-Seidel with $\omega = 1.2$ leads to divergence (not displayed in Table 3(a)) while the cell-based Vanka smoother is still almost unaffected by the variations of the relaxation parameter. Consequently, in terms of robustness the Vanka smoother should be preferred although the solution process takes longer in case of the isotropic and mildly anisotropic configurations. For the strongly anisotropic configuration the two solvers show comparable runtimes. Table 3(b) partially confirms this for the configuration CROSSOVER. Here, it is remarkable that MG-GS also fails for the 'standard' relaxation parameter $\omega = 1.0$ (not shown in Table 3(b)) and is much slower than MG-VANKA-C for the ANISO case.

In the mixed formulation setting we can also apply the two patch-based variants of the Vanka smoother. We do this for the same configurations as before and can make

Table 3: MG-GS vs. MG-VANKA-C; mixed formulation; $\nu = 0.3$. (a) ANALYTIC with aspect ratios 1, 4 and 16. (b) CROSSOVER-ISO/ANISO.

(a)

	MG-GS				MG-VANKA-C					
ω	0.8		1.0		0.8		1.0		1.2	
AR 1										
τ	1	2	1	2	1	2	1	2	1	2
lv 6	9	5	20	9	6	4	8	4	8	4
lv 7	9	5	21	9	6	4	8	4	8	4
lv 8	9	5	21	10	6	4	8	4	8	4
sec	41	44	96	88	113	131	129	131	113	128
AR 4										
τ	2	4	2	4	1	2	1	2	1	2
lv 6	33	16	23	11	18	10	17	9	17	10
lv 7	33	16	23	12	17	10	17	10	17	10
lv 8	32	16	23	12	18	10	17	10	17	10
sec	280	275	202	207	294	319	280	318	283	325
AR 16										
τ	16	32	16	32	4	8	4	8	4	8
lv 6	39	19	27	14	39	19	37	18	36	18
lv 7	45	23	33	16	42	21	40	20	39	20
lv 8	47	23	34	17	40	21	37	20	37	20
sec	3266	3100	2381	2296	2608	2744	2372	2566	2361	2606

(b)

	MG-GS				MG-VANKA-C					
ω	0.6		0.8		0.8		1.0		1.2	
iso										
τ	1	2	1	2	1	2	1	2	1	2
lv 3	28	16	20	12	9	6	8	6	8	6
lv 4	29	16	20	12	9	6	8	6	8	6
lv 5	28	16	19	12	8	6	8	6	8	6
sec	37	42	24	27	34	51	34	50	34	50
aniso										
τ	4	8	4	8	2	4	2	4	2	4
lv 3	17	9	11	7	7	5	7	5	7	5
lv 4	28	25	32	16	13	7	11	6	10	5
lv 5	126	63	82	41	27	14	23	12	22	11
sec	568	535	355	346	216	229	192	198	182	182

some interesting observations. For the simple ANALYTIC isotropic case it does again make not much sense to invest extra work into the smoothing process (Table 4(a)): Both patch-based variants are by far slower than (the optimal) MG-GS. Compared to the cell-based Vanka smoother they are slightly better in terms of iteration numbers, but only the diagonal patch-based Vanka smoother is able to reflect this also in to-

Table 4: MG-VANKA-PD vs. MG-VANKA-P; mixed formulation; $\nu = 0.3$ (a)ANALYTIC with aspect ratios 1, 4 and 16. (b) CROSSOVER-ISO/ANISO

(a)

	MG-VANKA-PD				MG-VANKA-P					
ω	0.8		1.0		0.8		1.0		1.2	
AR 1										
τ	1	2	1	2	1	2	1	2	1	2
lv 6	6	3	4	3	5	3	4	3	6	4
lv 7	6	3	4	3	5	3	5	3	6	4
lv 8	6	3	4	3	5	3	5	3	6	4
sec	127	126	84	126	157	191	161	192	188	251
AR 4										
τ	1	2	1	2	1	2	1	2	1	2
lv 6	12	7	15	9	7	4	6	4	7	4
lv 7	12	7	-	-	7	4	6	4	7	4
lv 8	12	7	-	-	7	4	7	4	7	5
sec	253	293			225	254	224	251	224	315
AR 16										
τ	2	4	2	4	1	2	1	2	1	2
lv 6	50	25	-	-	34	18	30	16	27	15
lv 7	55	28	-	-	37	20	33	18	30	17
lv 8	55	29	-	-	37	20	33	18	31	17
sec	2288	2636			1173	1256	1039	1155	1000	1089

(b)

	MG-VANKA-PD				MG-VANKA-P					
ω	0.6		0.8		0.8		1.0		1.2	
iso										
τ	1	2	1	2	1	2	1	2	1	2
lv 3	11	6	10	5	9	5	9	6	9	6
lv 4	11	6	10	5	9	5	9	5	9	6
lv 5	10	6	10	5	9	5	9	5	9	5
sec	51	60	52	50	70	76	69	76	70	76
aniso										
τ	2	4	2	4	1	2	1	2	1	2
lv 3	8	5	7	5	9	5	10	6	9	6
lv 4	18	9	14	7	9	5	9	6	9	6
lv 5	44	22	33	17	9	5	9	5	9	6
sec	442	438	332	338	67	76	69	76	69	90

tal computation time. The results for the anisotropic meshes in Table 4(a) show that for MG-VANKA-PD underrelaxation is clearly necessary, while MG-VANKA-P behaves quite robustly with respect to the relaxation parameter. (MG-VANKA-PD converges for AR 1 and $\omega = 1.2$, though, but it needs more iterations than with $\omega = 1.0$.) The computation times, too, show a clear superiority of MG-VANKA-P over all other smoothers despite being the most expensive one per smoothing step. This also holds for the CROSSOVER configuration as can be seen in Table 4(b). (MG-VANKA-PD diverges for $\omega = 1.0$ which is not shown in the table.) Here, it is especially worth mentioning that, in contrast to all other smoothers, the iteration number of MG-VANKA-P does *not* rise with increasing multigrid level and simultaneously increasing aspect ratio. A reason for this might be that the strong anisotropies of the two element layers around the holes are, so to speak, hidden in the direct solution of the patch-system with the full local displacement matrix.

4.3 Nearly incompressible material

In the remainder of the paper we will only deal with (nearly) incompressible material and, consequently, do not employ the pure displacement formulation anymore. So, we are now in a situation which resembles the incompressible flow setting and in which the Vanka-type smoothers should tap their full potential. Due to the LBB stabilisation terms the standard Gauß-Seidel smoother is still applicable also in the incompressible case such that we can continue to compare the different approaches. The configuration ANALYTIC is considered first. For MG-GS and MG-VANKA-C numbers for ω greater or equal 0.7 are not listed in Table 5(a), since for these values MG-GS diverges on all levels and MG-VANKA-C shows extremely slow or also no convergence.

So, for both smoothers a strong underrelaxation is mandatory to solve the problem at all. (We also tested $\omega = 0.2$, which showed worse results than $\omega = 0.4$.) Consequently, the number of iterations / smoothing steps are high compared to the compressible case, resulting in significantly longer computation times, especially in case of more anisotropic meshes. Again, for the isotropic case the Gauß-Seidel smoother seems to be sufficient, while the cell-based Vanka smoother is faster on anisotropic meshes. Regarding the relaxation parameter, the cell-based Vanka smoother shows a more irregular behaviour now: For ANALYTIC1 and ANALYTIC4 $\omega = 0.4$ is the better choice, while it is $\omega = 0.6$ for ANALYTIC16. For the Gauß-Seidel smoother, however, $\omega = 0.6$ always yields the best results. The results of the CROSSOVER configuration confirm these observations (see Table 5(b)).

Both smoothers, in summary, have severe problems to efficiently treat the anisotropic (nearly) incompressible case, so we have to examine if the patch-based Vanka smoothers perform better.

Looking at the number of iterations / smoothing steps and total CPU times in Tables 6(a) and 7(a), this is clearly the case. Even in the isotropic case they are now able to compete with the optimally tuned MG-GS in terms of CPU times, which was not true for the compressible configurations.

Table 5: MG-GS vs. MG-VANKA-C; mixed formulation; $\nu = 0.5$ and $\nu = 0.4999$, respectively. (a) ANALYTIC with aspect ratios 1, 4 and 16. (b) CROSSOVER-ISO/ANISO

(a)

	MG-GS				MG-VANKA-C			
ω	0.4		0.6		0.4		0.6	
AR 1								
τ	2	4	2	4	2	4	2	4
lv 6	18	10	17	11	8	7	21	9
lv 7	18	10	17	11	8	7	32	11
lv 8	18	10	17	11	8	7	33	11
sec	158	171	147	185	259	452	1072	723
AR 4								
τ	8	16	8	16	2	4	2	4
lv 6	22	12	13	9	17	9	21	9
lv 7	23	13	14	10	18	9	34	11
lv 8	24	13	14	11	18	10	31	14
sec	1028	914	597	772	589	655	1021	901
AR 16								
τ	64	128	64	128	16	32	16	32
lv 6	25	13	13	8	18	10	11	7
lv 7	27	15	18	10	17	11	13	8
lv 8	69	15	17	10	21	11	15	8
sec	18631	7933	4809	5640	5496	5838	3977	4308

(b)

	MG-GS				MG-VANKA-C			
ω	0.4		0.6		0.4		0.6	
iso								
τ	4	8	4	8	1	2	1	2
lv 3	13	8	9	7	15	9	16	7
lv 4	14	8	11	7	14	9	27	11
lv 5	14	9	15	8	14	9	46	18
sec	60	77	65	68	63	75	197	150
aniso								
τ	16	32	16	32	4	8	4	8
lv 3	8	6	6	5	6	5	6	5
lv 4	18	10	11	7	13	7	9	5
lv 5	46	24	28	14	29	15	19	10
sec	766	804	517	537	479	492	310	327

However, we have to perform underrelaxation here, as well, where a comparison with the compressible case is interesting: There, the *full* patch-based Vanka smoother is more robust with respect to the relaxation parameter than the *diagonal* variant, while here, in the incompressible case, *more* underrelaxation is necessary. For MG-VANKA-PD $\omega = 0.8$ seems to be a good choice, while it is between $\omega = 0.6$ and $\omega = 0.7$

Table 6: Mixed formulation; $\nu = 0.5$; configuration ANALYTIC with aspect ratios 1, 4 and 16. (a) MG-*, (b) BICG-MG-*.

(a)

	VANKA-PD				VANKA-P			
ω	0.6		0.8		0.6		0.7	
AR 1								
τ	1	2	1	2	1	2	1	2
lv 6	7	4	6	4	6	4	6	4
lv 7	7	4	5	4	6	4	6	3
lv 8	7	4	5	4	6	4	6	3
sec	146	167	105	167	190	256	197	195
AR 4								
τ	1	2	1	2	1	2	1	2
lv 6	17	9	14	7	8	5	7	5
lv 7	17	9	14	8	8	5	7	5
lv 8	17	9	14	8	8	5	7	5
sec	356	382	293	348	256	317	230	327
AR 16								
τ	4	8	4	8	2	4	2	4
lv 6	44	15	22	12	19	11	19	10
lv 7	>64	19	28	16	27	14	24	14
lv 8	-	21	30	17	>64	15	25	15
sec		3463	2482	2801	-	1913	1603	1913

(b)

	VANKA-PD				VANKA-P			
ω	0.6		0.8		0.6		0.7	
AR 1								
τ	1	2	1	2	1	2	1	2
lv 6	4	2	3	2	3	2	3	2
lv 7	4	2	3	2	3	2	3	2
lv 8	4	2	3	2	3	2	3	2
sec	153	173	110	174	163	258	162	261
AR 4								
τ	1	2	1	2	1	2	1	2
lv 6	6	4	5	4	4	3	4	3
lv 7	6	4	5	4	4	3	4	3
lv 8	6	4	5	4	3	3	4	3
sec	240	300	217	300	194	323	226	319
AR 16								
τ	4	8	4	8	2	4	2	4
lv 6	9	6	7	5	7	5	8	5
lv 7	11	6	9	6	8	5	8	6
lv 8	>32	7	10	7	16	7	10	6
sec		2214	1710	2223	2100	1681	1337	1532

Table 7: Mixed formulation; $\nu = 0.4999$; configurations CROSSOVER-ISO/ANISO. (a)MG-*, (b)BICG-MG-*.

(a)

	VANKA-PD				VANKA-P			
ω	0.6		0.8		0.6		0.7	
iso								
τ	1	2	1	2	1	2	1	2
lv 3	12	7	11	6	11	6	12	7
lv 4	12	6	11	6	10	5	12	6
lv 5	11	6	11	5	10	5	11	6
sec	57	61	56	50	76	76	84	98
aniso								
τ	1	2	1	2	1	2	1	2
lv 3	13	7	13	7	11	6	12	7
lv 4	30	16	23	12	10	5	12	6
lv 5	74	38	55	28	10	5	11	6
sec	367	382	282	281	77	76	85	91

(b)

	VANKA-PD				VANKA-P			
ω	0.6		0.8		0.6		0.7	
iso								
τ	1	2	1	2	1	2	1	2
lv 3	5	4	5	3	5	3	5	3
lv 4	5	4	4	3	4	3	5	3
lv 5	5	3	4	3	4	3	5	3
sec	47	61	41	50	61	91	70	93
aniso								
τ	1	2	1	2	1	2	1	2
lv 3	5	4	5	3	4	3	5	3
lv 4	7	5	7	4	4	3	5	3
lv 5	11	7	12	7	4	3	5	3
sec	114	141	125	131	62	76	70	92

for MG-VANKA-P. (The latter still converges for $\omega = 0.8$, though, but slightly worse than for $\omega = 0.7$, while MG-VANKA-PD diverges for $\omega = 1.0$, which is not shown in Tables 6(a) and 7(a).) That is why the superiority of the full variant over the diagonal one in case of anisotropic meshes is clearly observable, though, but not as striking as in the compressible situation.

BiCGstab as outer solver

A way to increase the robustness and the efficiency of multigrid is to use it not directly as solver but as a preconditioner within an outer iteration scheme. For this, we employ BICGSTAB and want to examine if this helps to better handle the above configurations. The relaxation parameters can be chosen as for the corresponding stand-alone MG solvers; only in rare cases different values lead to slightly better results.

When applying BICGSTAB as outer solver we can usually observe a decrease of iteration numbers of at least 50 percent compared to corresponding stand-alone MG solvers (see Table 6(a) vs. Table 6(b) and Table 7(a) vs. Table 7(b)). This is, of course, not surprising as BICGSTAB does two preconditioning steps per iteration. However, the interesting fact now is that for some configurations the iteration numbers decrease by far more than 50 percent. Especially, the performance of the *diagonal* patch-based Vanka smoother is significantly improved on anisotropic meshes. The solution of the CROSSOVER-ANISO configuration, for instance, takes less than half of the time. The *full* patch-based Vanka smoother clearly benefits from applying BICGSTAB, as well, even though the improvement is not as striking as for the diagonal variant.

The positive influence of BICGSTAB is even more crucial in case of the BEAM configuration. As mentioned in Section 4.1, the thin shape and the small Dirichlet boundary can lead to numerical difficulties. We can confirm this by comparing BEAM-ISO to the configuration CROSSOVER-ISO, both having a maximal element aspect ratio of roughly 3. Although CROSSOVER-ISO exhibits a more complicated geometry and irregular elements, less iterations are needed for convergence (compare Tables 7 and 8). The effect becomes even clearer for the BEAM-ANISO configuration. To solve the corresponding

Table 8: Mixed formulation; $\nu = 0.4999$; configurations BEAM-ISO/ANISO. (a)MG-*, (b) BICG-MG-*.

(a)

	VANKA-PD		VANKA-P	
ω	0.8		0.7	
iso				
τ	1	2	1	2
lv 5	17	9	12	7
lv 6	17	9	11	7
lv 7	16	8	11	7
sec	162	161	173	213
aniso				
τ	4	8	2	4
lv 6	394	208	213	121
lv 7	328	173	179	102
lv 8	281	148	156	88
sec	5765	6083	2453	2730

(b)

	VANKA-PD		VANKA-P	
ω	0.8		0.7	
iso				
τ	1	2	1	2
lv 5	6	4	6	3
lv 6	6	4	5	3
lv 7	6	4	5	3
sec	125	165	153	184
aniso				
τ	4	8	2	4
lv 6	27	18	24	15
lv 7	28	18	24	17
lv 8	29	17	24	15
sec	1196	1401	722	896

linear systems at all, we had to increase the maximal number of iterations (see Table 8, aniso). In terms of element aspect ratios a comparison to the ANALYTIC16 configuration (see Table 6) can be drawn. Considering MG-VANKA-PD on level 8 of BEAM-ANISO and on level 7 of ANALYTIC16, the latter is solved roughly 10 times faster. Comparing the results of MG-VANKA-P, one can observe a factor of roughly 6. (Of course, these large differences are also due to the fact that in the ANALYTIC16 configuration only *half* the elements exhibit the high aspect ratio.)

Now let us examine the influence of the outer BICGSTAB scheme in case of the BEAM configuration. Beginning with the isotropic beam, the BICG-variants show a degree of improvement which is similar to the configurations ANALYTIC4 and CROSSOVER-ISO (all three having similar maximal element aspect ratios). For the anisotropic beam configuration, however, we can make an interesting observation: Comparing the differences between Table 6(a) (AR 16, level 7) and Table 8(a) (aniso, level 8) with the corresponding differences between Table 6(b) and Table 8(b), one can observe that the above factors of 6 and 10, respectively, are decreased to roughly 3 for both Vanka variants. This means, that the difference in solving these two comparable configurations ANALYTIC16 and BEAM-ANISO significantly shrinks when multigrid is enclosed by an outer BICGSTAB scheme, i. e. the numerical problems arising with the beam configuration are considerably diminished.

Finite elasticity

To assess the Vanka smoothers in the context of finite elasticity we consider the BLOCK configuration. Applying the two loads $(0, -20)$ and $(0, -300)$, leads to different compression rates of the block and thus to different nonlinearities. Fig. 7 shows the resulting deformation and the von Mises stress.

In case of the higher load, line search for the Newton-Raphson schemes becomes necessary. We consider two different coarse grids of the block configuration, exhibiting aspect ratios of 1 and 4, respectively (see Fig. 6(a)). For the linear solvers we only use the patch-based Vanka smoothers as the others already had problems dealing

Table 9: Total number of linear iterations for MG-VANKA-PD, MG-VANKA-P, BICG-MG-VANKA-PD, BICG-MG-VANKA-P; finite deformation; mixed formulation; configuration BLOCK; load -20 and -300 (for the smaller load 3 Newton iterations were performed, for the higher load 7 Newton iterations). (a) load -20, (b) load -300.

(a)

	MG-		BICG-MG-	
	V.-PD	V.-P	V.-PD	V.-P
BLOCK-ISO, $\tau = 1$				
ω	0.7	0.5	0.7	0.5
lv 5	8	9	5	5
lv 6	8	9	5	5
lv 7	8	9	5	5
sec	78	136	79	122
BLOCK-ANISO				
ω	0.8	0.5	0.7	0.5
τ	1	1	1	1
lv 4	16	11	7	5
lv 5	14	11	7	6
lv 6	14	11	7	5
sec	137	166	121	139

(b)

	MG-		BICG-MG-	
	V.-PD	V.-P	V.-PD	V.-P
BLOCK-ISO, $\tau = 1$				
ω	0.7	0.5	0.5	0.4
lv 5	17	17	10	9
lv 6	17	17	10	9
lv 7	17	18	10	9
sec	165	272	167	260
BLOCK-ANISO				
ω	0.6	0.6	0.5	0.5
τ	4	2	1	1
lv 4	34	24	27	18
lv 5	34	21	32	14
lv 6	32	20	26	15
sec	1220	601	475	426

with the *linear* incompressible case. The nonlinear iteration is stopped when the initial residual norm is decreased by a factor of 10^{-5}, the linear solvers use a relative stopping criterion of $\varepsilon_{\text{rel}} = 10^{-2}$. Table 9 shows the total number of linear iterations. For the small load always three Newton steps are performed, for the high load seven Newton steps. The given times are the accumulated linear solving times on the finest level, matrix assembling times are not contained. In most cases, performing exactly one smoothing step is the best choice. Only for the MG solvers in the case of the anisotropic block under higher load the number of smoothing steps had to be increased. For each configuration we tested the relaxation parameters $\omega = 0.4, 0.5, \ldots, 0.8$, but for sake of clarity we only show the one that performed best, respectively. In the following evaluation we comment on the solvers' robustness with respect to the relaxation parameter.

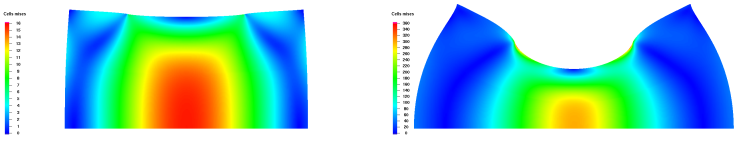

(a) (b)

Figure 7: Configuration BLOCK under two different loads (von Mises stress displayed). (a) Load $(0, -20)$, (b) Load $(0, -300)$.

Most of the observations made for the linear test cases are confirmed in the finite deformation setting. We first consider the results for the isotropic block (see the upper parts of Tables 9(a) and (b)). For both loading states the diagonal variant of the patch-based Vanka smoother outperforms the full Vanka smoother in terms of runtimes, while they need roughly the same number of iterations. At least for the full Vanka smoother the outer BICGSTAB scheme slightly improves the efficiency. Both

smoother variants are robust with respect to the relaxation parameter ω within the tested interval, only the full Vanka variant deteriorates for $\omega = 0.8$ (not shown in the table).

For the anisotropic block we get different results (see lower parts of Tables 9(a) and (b)): In case of the small load, the diagonal Vanka smoother is still slightly faster, though, but it needs more iterations than the full variant. In case of the second loading state, however, the full Vanka smoother is clearly superior to the diagonal one, in terms of iteration numbers, runtimes, and especially robustness: MG-VANKA-PD diverges when only one or two smoothings steps are applied, and both, MG-VANKA-PD and BICG-MG-VANKA-PD, diverge for relaxation parameters $\omega = 0.7$ and $\omega = 0.8$, independent of the number of smoothing steps. MG-VANKA-P, however, shows robust convergence behaviour for $\omega \in [0.4, 0.8]$ with two smoothing steps already and converges in case of one smoothing step at least for $\omega = 0.4$. BICG-MG-VANKA-P needs only one smoothing step to converge robustly for all tested relaxation parameters. (Again, the full Vanka variants slightly deteriorate for $\omega = 0.8$.) The positive influence of the outer BICGSTAB scheme is much more significant for the anisotropic block than for the isotropic one, especially for the high loading state, where – similar to the small deformation case – the diagonal Vanka variant benefits more than the full Vanka variant.

A comparison between the two block configurations with respect to the applied surface force is interesting. For the small loading state the full Vanka smoother shows only slight runtime differences between the isotropic and the anisotropic block, i. e. factors of 1.2 and 1.1 for MG-VANKA-P and BICG-MG-VANKA-P, resp. For the high surface force, these factors increase to 2.2 and 1.6, resp. For the diagonal Vanka smoother, however, the dependence on the applied force is much more significant: While in case of the smaller load the runtime of MG-VANKA-PD to solve the anisotropic configuration is 1.8 times as high as for the isotropic one, it is 7.4 times as high in case of the higher load. For BICG-MG-VANKA-PD the runtime differences increase from 1.1 to 2.8.

In summary, the test cases considered here indicate that both, the diagonal and the full Vanka smoother are in principle able to handle large deformations. The difficulties of the diagonal Vanka variant with higher aspect ratios seem to be amplified in the presence of the resulting nonlinearities. The full Vanka variant, however, is capable to robustly deal with the combined effects of strong nonlinearities and higher aspect ratios.

5 Summary

In this paper we described the use of Vanka-like multigrid smoothers in the context of Q_1/Q_1 finite element simulations in Computational Solid Mechanics. We presented and compared four smoother types that are frequently considered in (CFD-) literature. From the numerical tests we can draw the following main conclusions:

- All presented smoothers show a certain degree of sensitivity with respect to the

relaxation parameter ω. A value that is optimal for one configuration may lead to divergence in a different configuration. Consequently, a proper choice of this parameter cannot be done automatically and requires some experience by the user. This has to be seen as general drawback of *all* considered smoothers.

- For compressible material and fairly isotropic meshes the standard Gauß-Seidel smoother provides good results and is often the most efficient. But as soon as mesh anisotropies and/or incompressibility are involved it is advantageous or even necessary to switch to one of the more sophisticated Vanka smoothers.
- The observation already made by other authors that the diagonal patch-based Vanka smoother shows deficiencies on anisotropic meshes is clearly confirmed. *But:* When the multigrid scheme is enclosed by an outer BICGSTAB (or similar) method, this effect is significantly weakened. However, none of the presented smoothers is robust with respect to higher aspect ratios as the comparisons between isotropic and anisotropic meshes show.
- For incompressible material it is mandatory to use one of the patch-based Vanka smoothers. The standard Gauß-Seidel and the cell-based Vanka smoother have to be strongly underrelaxed and solve only very simple, isotropic configurations in reasonable time.
- Instead of using multigrid as stand-alone solver it is recommendable to apply it as preconditioner of an outer Krylov space method. In many cases, robustness and efficiency of the overall solving process are considerably increased as, for instance, the BEAM configuration shows.

Future work has to focus on both, theoretical and practical aspects of Vanka-type smoothing in elasticity. Often, the main difficulty in the convergence theory of multigrid schemes is to prove the smoothing property [8, 29]. Following the ideas of Klawonn, Widlund and Pavarino who present theoretical results on domain decomposition methods in elasticity (see references [16, 25, 37] for an overview of their work), could be instructive to at least show that Vanka is an efficient solver. In this case, multigrid convergence is ensured as long as enough Vanka smoothing steps are performed. From the practical point of view, the most important step in future work is the application of the aforementioned lining- and patching-strategies to increase the smoothers' robustness against mesh anisotropies. Furthermore, Vanka-type smoothers will be compared to globally working (decoupled) smoothers/preconditioners for saddle point systems. For this comparison, not only the numerical efficiency will be assessed, but also the parallel efficiency in a multi-processor computer environment. Other relevant topics are the inclusion of transient simulations into the test environment and the application of the Vanka idea in connection with EAS (Enhanced Assumed Strains) elements, which are very popular in the CSM community.

Acknowledgments

This work has been supported by DFG, under grant TU 102/11-3.

References

[1] F. ARMERO, *On the locking and stability of finite elements in finite deformation plane strain problems*, Comp. and. Struct., 75 (2000), pp. 261-290.

[2] I. BABUŠKA AND M. SURI, *Locking effects in the finite element approximation of elasticity problems*, Numerische Mathematik, 62(1992), pp. 439-463.

[3] R. BECKER, *An Adaptive Finite Element Method for the Incompressible Navier–Stokes Equations on Time-Dependent Domains*. PhD thesis, Universität Heidelberg, 1995.

[4] M. BENZI AND M. OLSHANSKII, *An augmented Lagrangian-based approach to the Oseen-problem*, SIAM Journal on Scientific Computing, 28(6) (2006), pp. 2095-2113.

[5] P. B. BOCHEV AND M. D. GUNZBURGER, *An absolutely stable pressure-poisson stabilized finite element method for the Stokes equations*, SIAM Journal on Numerical Analysis, 47(3) (2004), pp. 1189-1207.

[6] P. B. BOCHEV, M. D. GUNZBURGER, AND R. B. LEHOUCQ, *On stabilized finite element methods for the Stokes problem in the small time step limit*, International Journal for Numerical Methods in Fluids, 53 (2007), pp. 573-597.

[7] D. BRAESS, Finite Element, Springer, Berlin, 3rd edition, 2003.

[8] D. BRAESS AND R. SARAZIN, *An efficient smoother for the Stokes problem*, Applied Numerical Mathematics, 23 (1997), pp. 3-20.

[9] F. J. GASPAR, F. J. LISBONA, C. W. OOSTERLEE, AND R. WIENANDS, *A systematic comparison of coupled and distributive smoothing in multigrid for the poroelasticity system*, Num. Lin. Alg. with Appl., 11 (2004), pp. 93-113.

[10] W. HACKBUSCH, Multi-Grid Methods and Applications, Springer Series in Computational Mathematics. Springer, Berlin, 1985.

[11] J. HRON AND S. TUREK, *A monolithic FEM solver for an ALE formulation of fluid structure interaction with configurations for numerical benchmarking*, In M. Papadrakakis, E. Onate, and B. Schrefler, editors, *Computational Methods for Coupled Problems in Science and Engineering*, Proceedings 'First International Conference on Computational Methods for Coupled Problems in Science and Engineering' (Santorini, May 25th - 27th), 2005.

[12] V. JOHN, *A comparison of parallel solvers for the incompressible Navier-Stokes equations*, Computing and Visualization in Science, 4 (1999), pp. 193-200.

[13] V. JOHN, *Higher order finite element methods and multigrid solvers in a benchmark problem for the 3D Navier-Stokes equations*, International Journal for Numerical Methods in Fluids, 40 (2002), pp. 775-798.

[14] V. JOHN AND G. MATTHIES, *Higher order finite element discretizations in a benchmark problem for incompressible flows*, International Journal for Numerical Methods in Fluids, 37 (2001), pp. 885-903.

[15] V. JOHN AND L. TOBISKA, *Numerical performance of smoothers in coupled multigrid methods for the parallel solution of the incompressible Navier-Stokes equations*, International Journal for Numerical Methods in Fluids, 33 (2000), pp. 453-473.

[16] A. KLAWONN, `http://www.uni-due.de/numerik/publications.shtml`, List of publications.

[17] M. KÖSTER, *Robuste Mehrgitter-Krylowraum-Techniken für FEM-Verfahren*, 2004. Diplomarbeit, Universität Dortmund.

[18] M. LARIN AND A. REUSKEN, *A comparative study of efficient iterative solvers for generalized Stokes equations*, Numerical Linear Algebra with Applications, 15 (2008), pp. 13-34.

[19] P. LE TALLEC, *Numerical methods for nonlinear three-dimensional elasticity*, In P. G. Ciarlet and J. L. Lions, editors, Handbook of Numerical Analysis, volume III, pp. 465-662. North-

Holland, 1994.

[20] S. MANSERVISI, *Numerical analysis of Vanka-type solvers for steady Stokes and Navier-Stokes flows*, SIAM Journal on Numerical Analysis, 44(5) (2006), pp. 2025-2056.

[21] J. MOLENAAR, *A two-grid analysis of the combination of mixed finite elements and Vanka-type relaxation*, In W. Hackbusch and U. Trottenberg, editors, Multigrid Methods III, Proc. 3rd Eur. Conf., Bonn/Germany, ISNM 98, pp. 313-323. Birkhäuser Verlag, 1991.

[22] A. OUAZZI AND S. TUREK, *Efficient multigrid and data structures for edge-oriented FEM stabilization*, Numerical Mathematics and Advanced Applications Enumath 2005, pp. 520-527. Springer, Berlin, 2006. ISBN-10 3-540-34287-7.

[23] E. E. OVTCHINNIKOV AND L. S. XANTHIS, *Iterative subspace correction methods for thin elastic structures and Korn's type inequality in subspaces*, Proceedings: Mathematical, Physical and Engineering Sciences, 454 (1976), pp. 2023-2039, 1998.

[24] S. V. PATANKAR AND D. B. SPALDING, *A calculation procedure for heat and mass transfer in three-dimensional parabolic flows*, Int. J. Heat Mass Transfer, 15 (1972), pp. 1787-1806.

[25] L. F. PAVARINO. `http://newrobin.mat.unimi.it/users/pavarino/CV_eng.pdf`, List of publications.

[26] S. REESE, M. KÜSSNER, AND B. D. REDDY, *A new stabilization technique for finite elements in finite elasticity*, International Journal for Numerical Methods in Engineering, 44 (1999), pp. 1617-1652.

[27] F. SCHIEWECK, *Parallele Lösung der stationären, inkompressiblen Navier–Stokes Gleichungen*, 1997. Habilitation, Otto-von-Guericke Universität Magdeburg, Fakultät Mathematik.

[28] R. SCHMACHTEL, Robuste lineare und nichtlineare Lösungsverfahren für die inkompressiblen Navier–Stokes-Gleichungen. PhD thesis, Universität Dortmund, June 2003.

[29] J. SCHÖBERL AND W. ZULEHNER, *On Schwarz-type smoothers for saddle point problems*, Numerische Mathematik, 95 (2003), pp. 377-399.

[30] F. T. SUTTMEIER, *An adaptive displacement/pressure finite element scheme for treating incompressibility effects in elasto-plastic materials*, Numerical Methods for Partial Differential Equations, 17 (2001), pp. 369-382.

[31] M. C. THOMPSON AND J. H. FERZIGER, *An adaptive multigrid technique for the incompressible Navier-Stokes equations*, J. Comput. Phys., 82 (1989), pp. 94-121.

[32] S. TUREK, Efficient Solvers for Incompressible Flow Problems: An Algorithmic and Computational Approach. Springer, Berlin, 1999.

[33] S. TUREK AND M. SCHÄFER, *Benchmark computations of laminar flow around cylinder*, In E. H. Hirschel, editor, Flow Simulation with High-Performance Computers II, volume 52 of *Notes on Numerical Fluid Mechanics*, pp. 547-566. Vieweg, 1996. co. F. Durst, E. Krause, R. Rannacher.

[34] H. A. VAN DER VORST, *Bi-CGSTAB: A fast and smoothly converging variant of Bi-CG for the solution of nonsymmetric linear systems*, *SIAM Journal on Scientific and Statistical Computing*, 13(2) (1992), pp. 631-644.

[35] S. P. VANKA, *Block-implicit multigrid solution of Navier-Stokes equations in primitive variables*, J. Comput. Phys., 65 (1986), pp. 138-158.

[36] P. WESSELING AND C. W. OOSTERLEE, *Geometric multigrid with applications to computational dynamics*, J. Comput. Appl. Math., 128 (2001), pp. 311-334.

[37] O. B. WIDLUND, `http://www.cs.nyu.edu/widlund/papers.html`, List of publications.

[38] S. ZENG AND P. WESSELING, *Numerical study of a multigrid method with four smoothing methods for the incompressible Navier-Stokes equations in general coordinates*. In N. D. Melson, Th. A. Manteuffel, and S. F. McCormick, editors, Sixth Copper Mountain Conference on Multigrid Methods, pp. 691-708. NASA Langley Research Center, November 1993.